

# Collaborative Edge-to-Server Inference for Vision-Language Models

Soochang Song and Yongjune Kim, *Member, IEEE*

arXiv:2512.16349v1 [cs.CV] 18 Dec 2025

**Abstract**—We propose a collaborative edge-to-server inference framework for vision-language models (VLMs) that reduces the communication cost while maintaining inference accuracy. In typical deployments, visual data captured at edge devices (clients) is transmitted to the server for VLM inference. However, resizing the original image (global image) to match the vision encoder’s input resolution often discards fine-grained details, leading to accuracy degradation. To overcome this limitation, we design a two-stage framework. In the first stage, the server performs inference on the global image and identifies a region of interest (RoI) using the VLM’s internal attention. The min-entropy of the output tokens is then computed as a confidence measure to determine whether retransmission is required. If the min-entropy exceeds a predefined threshold, the server requests the edge device to send a detail-preserved local image of the RoI. The server then refines its inference by jointly leveraging the global and local images. This selective retransmission strategy ensures that only essential visual content is transmitted. Experiments across multiple VLM architectures show that the proposed framework significantly reduces communication cost while maintaining inference accuracy.

**Index Terms**—Edge-to-server inference, collaborative inference, multimodal semantic communications, attention-aware visual cropping, entropy-aware image retransmission, vision-language models (VLMs).

## I. INTRODUCTION

With the rapid advancement of artificial intelligence (AI), the integration of multiple data modalities—such as images, text, and audio—into a shared embedding space has become a central paradigm in modern AI systems [1]–[3]. Among these, vision-language models (VLMs), also referred to as multimodal large language models (MLLMs), have emerged as a prominent and widely adopted architecture, combining a vision encoder with a large language model (LLM) to enable visual reasoning capabilities [3]–[5]. This architecture facilitates complex multimodal tasks that require joint understanding of visual and textual inputs, including visual question answering (VQA), image captioning, and image-text retrieval [6].

In real-world applications, VLMs are often required to process visual data captured at edge devices (clients). However, deploying a full VLM directly on the edge is generally infeasible due to its substantial computation and memory costs [7], [8]. Consequently, the visual data is typically transmitted to a server hosting the VLM for inference. To match the input resolution requirements of the vision encoder (e.g.,  $336 \times 336$  pixels) [1], [9], [10], the original images can be

S. Song and Y. Kim are with the Department of Electrical Engineering, Pohang University of Science and Technology (POSTECH), Pohang 37673, South Korea (e-mail: {ssc6351, yongjune}@postech.ac.kr).

resized before transmission. While resizing reduces communication cost, it may discard fine-grained visual information, particularly in high-resolution images, thereby degrading inference accuracy [11]. Alternatively, one may transmit the full-resolution image without downscaling, which preserves details but significantly increases communication load.

To address this problem, our framework introduces an uncertainty-aware retransmission mechanism tailored to the collaborative edge-to-server setting. In the first stage, the edge device transmits a low-resolution global image along with the question to the server. The server performs an initial inference and quantifies inference uncertainty using the min-entropy of the output tokens. If the min-entropy is below a predefined threshold, the inference result is directly finalized. Otherwise, a second stage is triggered: the server leverages the VLM’s internal attention scores to identify a task-relevant region of interest (RoI) and requests a detail-preserved local image from the edge device. Upon receiving the retransmission request, the edge device extracts the local image from the original image and transmits it to the server. The server then refines its inference by jointly processing the global and local images. This uncertainty-aware, two-stage strategy reduces communication overhead by transmitting task-relevant high-quality visual details only when necessary, while maintaining inference accuracy across diverse tasks.

At the core of the proposed framework is an entropy-aware decision mechanism that determines whether retransmission is required based on the VLM’s inference uncertainty. Since the server cannot directly ascertain whether the initial inference is correct, uncertainty is estimated from output probabilities and used as a proxy. Specifically, we compute the per-token min-entropy from the softmax outputs of the LLM decoder at each generation step and average it across all output tokens to obtain a single scalar decision statistic. This enables the server to request a local image only when the initial inference is likely unreliable, thereby attaining accuracy comparable to unconditionally transmitting local details while substantially reducing communication overhead.

Moreover, the proposed framework also alleviates server-side computational overhead compared with conventional schemes that either perform inference on higher-resolution images transmitted from the edge or always transmit an additional local image after the global image for inference. In VLMs, the LLM decoder accounts for the majority of overall floating-point operations (FLOPs). Since the number of visual tokens typically dominates the total number of input tokens in VQA tasks, the computational complexity of the VLM scales approximately linearly with the number of visual tokens [12].

By selectively increasing the number of visual tokens only when necessary, the min-entropy-based retransmission strategy significantly reduces the server-side computational cost while maintaining inference accuracy.

Experimental results show that decisions guided by min-entropy [13] achieve higher inference accuracy than those based on other uncertainty metrics such as Shannon entropy [14] and probability margin [15]. Compared to high-resolution end-to-end models such as LLaVA-1.5-HD [3], the proposed framework provides a more favorable tradeoff between inference accuracy and both communication and computation costs. In addition, it is complementary to image compression techniques, enabling further communication efficiency and remaining broadly applicable across diverse VLM architectures.

The primary contributions of this work are summarized as follows:

- We propose a collaborative edge-to-server inference framework for VLMs that improves inference accuracy by jointly leveraging a global image and a local image that preserves task-relevant details.
- We introduce an entropy-aware retransmission mechanism that minimizes unnecessary data transmission by triggering local image requests only under high inference uncertainty, thereby reducing communication overhead without degrading accuracy.
- We demonstrate the effectiveness and generalizability of the proposed framework through extensive experiments on multiple VLM architectures and datasets, validating its robustness and practical applicability.

The rest of this paper is organized as follows. Section II provides an overview of the VLM architecture with attention mechanism, and Section III introduces related work. Section IV details our edge-to-server inference framework. Section V and Section VI present our main contributions, which include entropy-aware image retransmission and attention-guided collaborative visual cropping, respectively. Section VII provides experimental results, followed by conclusions in Section VIII.

## II. BACKGROUND

### A. Vision-Language Models

VLMs integrate visual and linguistic inputs within a unified transformer architecture and typically consist of two components: a vision encoder [1] and an LLM decoder [16]–[18]. A simplified overview of the VLM architecture is shown in Fig. 1.

The model takes as input an image-text pair  $(I, S)$ , where  $I \in \mathbb{R}^{h \times w \times 3}$  denotes an original RGB image in the pixel domain and  $S$  denotes a natural language sentence (e.g., a question referring to the image in a VQA task). Here,  $h$  and  $w$  represent the height and width of the original image, respectively. The image  $I$  is first resized to a fixed resolution  $\hat{I} \in \mathbb{R}^{\hat{h} \times \hat{w} \times 3}$  to align with the input resolution of the vision encoder, where  $\hat{h}$  and  $\hat{w}$  denote the height and width of the encoder's input. The vision encoder  $f_v(\cdot)$  consists of two modules: a Vision Transformer (ViT) [1], [9] and a multimodal

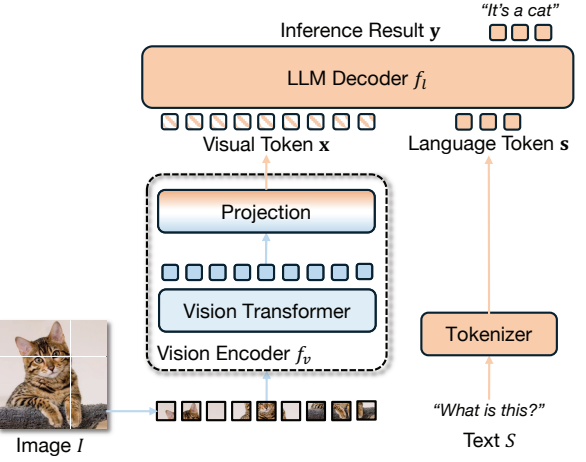


Fig. 1. Overview of the VLM architecture [3].

projection layer [3], [4]. The ViT divides the image into square patches and extracts visual features. The multimodal projector then maps these features into the shared embedding space of the LLM by producing visual tokens  $\mathbf{x} \in \mathbb{R}^{n_v \times d_{LLM}}$ , where  $n_v$  and  $d_{LLM}$  denote the number of visual tokens and the hidden dimension of the LLM, respectively. The visual encoding process can be expressed as

$$\mathbf{x} = f_v(\hat{I}). \quad (1)$$

The text input  $S$  is tokenized using a pretrained tokenizer [19], yielding a sequence of language tokens:

$$\mathbf{s} = \text{Tokenize}(S), \quad (2)$$

where  $\mathbf{s} \in \mathbb{R}^{n_s \times d_{LLM}}$  and  $n_s$  denotes the number of language tokens. Given the visual tokens  $\mathbf{x}$ , language tokens  $\mathbf{s}$ , and previously generated outputs  $\mathbf{y}_{<t}$ , the LLM decoder  $f_l(\cdot)$  generates the output token  $y_t$  autoregressively:

$$y_t = f_l(\mathbf{x}, \mathbf{s}, \mathbf{y}_{<t}), \quad (3)$$

where  $y_t \in \mathbb{R}^{d_{LLM}}$  represents the output token generated at step  $t$ . The final sequence  $\mathbf{y} = \{y_1, \dots, y_T\}$  is then detokenized [19] to produce the natural language output, where  $T$  denotes the total number of decoding steps.

### B. Attention Mechanism

Transformer layers in both the visual encoder and LLM decoder rely on the multi-head self-attention (MHSA) mechanism, though there are subtle differences in how it is applied. Given an input sequence  $\mathbf{z} \in \mathbb{R}^{n \times d}$ , where  $n$  denotes the sequence length and  $d$  denotes the transformer dimension. The query, key, and value matrices are computed through linear projections:

$$[Q, K, V] = \mathbf{z}U_{QKV}, \quad U_{QKV} \in \mathbb{R}^{d \times 3d_H}, \quad (4)$$

where  $Q, K, V \in \mathbb{R}^{n \times d_H}$ , and  $d_H = d/H$  denotes the per-head dimension with  $H$  attention heads.

In the ViT, unmasked self-attention is applied, and the attention weight matrix is computed as:

$$A = \text{softmax} \left( \frac{QK^\top}{\sqrt{d_H}} \right). \quad (5)$$

In contrast, the LLM decoder employs masked self-attention [20] to preserve the autoregressive property of language modeling. A lower triangular mask  $M \in \mathbb{R}^{n \times n}$  is added to prevent tokens from attending to future positions:

$$A = \text{softmax} \left( \frac{QK^\top + M}{\sqrt{d_H}} \right). \quad (6)$$

The self-attention output is then given by

$$\text{SA}(\mathbf{z}) = AV. \quad (7)$$

The MHSA mechanism extends this operation by computing  $H$  parallel self-attention outputs and concatenating them:

$$\text{MHSA}(\mathbf{z}) = [\text{SA}_1(\mathbf{z}), \dots, \text{SA}_H(\mathbf{z})] U_{\text{MHSA}}, \quad (8)$$

where  $U_{\text{MHSA}} \in \mathbb{R}^{d \times d}$  is the projection matrix for the MHSA output.

The attention weight matrix  $A$  provides interpretability by indicating which input tokens the model focuses on when responding to a given query. The choice of query for attention analysis depends on the task and the model architecture. For image classification using ViTs, the class token typically serves as the query [9], [21], [22]. In contrast, for language modeling in LLMs or VLMs, the generated output tokens can serve as the queries that attend to the encoded inputs [11], [23], [24].

### III. RELATED WORK

#### A. Multimodal Semantic Communications

With the rapid advancement of AI, the paradigms of semantic and task-oriented communications, which focus on extracting and transmitting only task-relevant information, have garnered significant attention. Unlike conventional approaches that focus on bit- or symbol-level fidelity, these approaches aim to maintain semantic fidelity and task performance [25]–[29]. Recent progress in multimodal AI has further expanded the potential of semantic communication. For instance, [30] proposes a transformer-based framework that independently encodes text, image, and audio modalities before feeding them into a unified decoder, thereby leveraging cross-modal relationships to improve communication efficiency.

Several studies have explored the integration of VLMs into communication systems. For example, [7] proposes a collaborative inference framework that deploys the vision encoder on an edge device and the language model decoder on a server. To reduce the communication cost of high-resolution images, they employ vector quantization and neural compression on the extracted visual features. The authors of [8] leverage VLM-derived ROI information to extract a subset of image regions from video frames, effectively reducing the bandwidth required for transmission. While these approaches demonstrate the feasibility of integrating VLMs into communication systems, they often require non-trivial computation on edge devices. In contrast, our framework performs most computations on the server, imposing minimal computational and power burden on the edge device.

#### B. Uncertainty Estimation in AI Inference

As AI models are increasingly deployed in critical domains such as biomedicine, security, and autonomous systems, assessing and mitigating the risks of hallucinations and erroneous predictions has become imperative [31]. To address this challenge, a growing body of research focuses on quantifying model uncertainty as a proxy for inference reliability. In natural language processing (NLP), token-level uncertainty estimation has been extensively investigated. For example, [32], [33] quantify the uncertainty of a generated sentence based on the probability distribution over output tokens. Building upon these efforts, we propose an edge-to-server collaborative inference framework for multimodal tasks, in which uncertainty-aware retransmission effectively reduces communication cost while maintaining inference accuracy.

In the context of semantic communications, [21] applies uncertainty estimation to collaborative edge-to-server inference for image classification. Specifically, the entropy of the softmax output from the ViT classification head is used to decide whether the prediction of a lightweight edge model should be accepted or whether the image should be transmitted to the server for more reliable inference. Beyond image classification, our work builds upon the underlying principle of uncertainty-aware collaborative inference and reformulates it for VLMs, introducing an uncertainty-aware retransmission strategy that effectively reduces communication cost for various VQA tasks.

### IV. COLLABORATIVE EDGE-TO-SERVER INFERENCE FRAMEWORK FOR VISION-LANGUAGE MODELS

We propose a collaborative edge-to-server inference framework built on pre-trained, off-the-shelf VLMs. The proposed framework incorporates entropy-aware image retransmission and attention-guided collaborative visual cropping inspired by [11] to reduce communication cost while maintaining inference accuracy. In this setting, each client uses an edge device connected to the server over a communication channel. The inference task is performed on input data residing on the edge device, consisting of visual images and textual questions posed by the client. Due to the substantial computational and memory demands of modern VLMs, it is infeasible to deploy and execute the full model directly on the edge device. Hence, the image data should be transmitted to the server hosting the VLM. To meet the input resolution of the vision encoder, which is often lower than that of the original image, the image can be downsampled before transmission; however, this process may remove fine-grained visual details and degrade inference accuracy. Alternatively, transmitting the full-resolution image preserves those details but drastically increases communication overhead.

To address this problem, we introduce a two-stage image transmission and inference protocol between the edge device and the server. As shown in Fig. 2, the proposed framework achieves communication efficiency by adaptively balancing communication cost and inference accuracy through uncertainty-aware retransmission and attention-guided refinement.

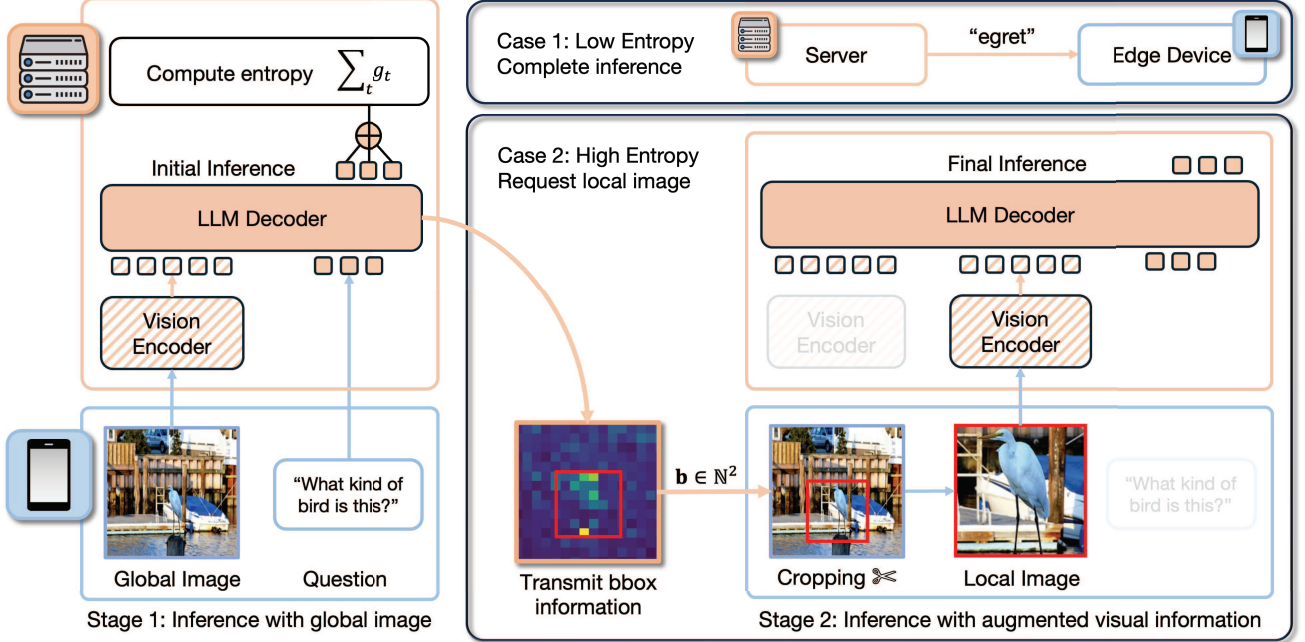


Fig. 2. Overview of the proposed two-stage collaborative edge-to-server inference framework. The edge device first transmits a global image to the server for initial inference. If high uncertainty is detected in the output token distribution, the server requests a local image based on an attention-derived bounding box. The edge device then crops the corresponding region from the original image and transmits it to the server. The server performs refined inference using both global and local visual features.

In the proposed framework, the edge device first transmits a visual input (i.e., a global image obtained by downscaling the original image) and a textual input (i.e., a question posed by the client) to the server. Upon receiving both inputs, the server-side VLM performs an initial inference. During inference, the server estimates the uncertainty of its prediction using the min-entropy of the output distribution of the server model. If the min-entropy is low, indicating high confidence, the inference result is finalized and transmitted to the edge device. Conversely, if the min-entropy is high, a secondary stage is triggered.

In the second stage, the server computes a relative attention map over the global image to identify the VLM’s RoI. The relative attention map is obtained by normalizing the raw attention weights extracted from the LLM decoder with a generic attention map acquired by a generic prompt [11]. Based on this relative attention map, the server identifies the position of the bounding box that exhibits the highest attention activation. The bounding box information is then transmitted to the edge device, along with a request for a detailed local image. The edge device crops the original image according to the received bounding box information, generating a local image that contains high-quality details of semantically important regions. This local image is transmitted to the server, where it is concatenated with the tokens of the global image to perform a second, more accurate inference. The refined answer is finally returned to the edge device.

The overall process is summarized in Algorithm 1. On the edge device, given the  $i$ -th image–text pair  $(I^{(i)}, S^{(i)})$ , the image is resized to match the VLM input resolution:  $\hat{I}^{(i)} = \text{Resize}(I^{(i)})$ . The resized image  $\hat{I}^{(i)}$  and the corresponding sentence  $S^{(i)}$  are then transmitted to the server.

Upon receiving these inputs, the server extracts the global visual feature  $\mathbf{x}^{(i)} = f_v(\hat{I}^{(i)})$  and encodes the input sentence  $\mathbf{s}^{(i)} = \text{Tokenize}(S^{(i)})$ . The autoregressive language model  $f_l(\cdot)$  subsequently generates a sequence of output tokens  $\mathbf{y}^{(i)} = \{y_1^{(i)}, \dots, y_T^{(i)}\}$ , conditioned on the encoded inputs and previously generated tokens.

During decoding, the server measures the token-level uncertainty using an entropy function  $g(\cdot)$ . The average entropy across the output sequence is computed as:

$$G_{\text{avg}} = \frac{1}{T} \sum_{t=1}^T g(\mathbf{x}^{(i)}, \mathbf{s}^{(i)}, \mathbf{y}_{<t}^{(i)}). \quad (9)$$

If  $G_{\text{avg}} \geq \eta$ , where  $\eta$  denotes a predefined uncertainty threshold, the server triggers a second stage and computes the relative attention map  $A_{\text{rel}}^{(i)}$ :

$$A_{\text{rel}}^{(i)} = \text{Rel\_Att}(\mathbf{x}^{(i)}, \mathbf{s}^{(i)}). \quad (10)$$

This map identifies the RoI that receives the highest model attention during generation. The server then determines a bounding box corresponding to the RoI and transmits its information vector  $\mathbf{b}^{(i)} = [b_1^{(i)}, b_2^{(i)}]^\top$  to the edge device:

$$\mathbf{b}^{(i)} = \text{Find\_Bbox}(A_{\text{rel}}^{(i)}), \quad (11)$$

where  $b_1^{(i)}, b_2^{(i)} \in \mathbb{N}$  denote the index of the visual token corresponding to the top-left coordinate of the bounding box and the side length of the square-shaped bounding box, respectively.

After receiving a retransmission request, the edge device crops the original image according to  $\mathbf{b}^{(i)}$  to obtain a local image and transmits it to the server. The server encodes the

---

**Algorithm 1** Proposed Collaborative Edge-to-Server Inference Framework
 

---

**Input:** A set of image and text pairs  $\{(I^{(1)}, S^{(1)}), \dots, (I^{(n)}, S^{(n)})\}$ .  
**Output:** Corresponding generated outputs  $\{y^{(1)}, \dots, y^{(n)}\}$ .

```

1: for  $i = 1 : n$  do
2:   # Edge Device
3:    $\hat{I}^{(i)} \leftarrow \text{Resize}(I^{(i)})$                                       $\triangleright$  Resize image to match the VLM input resolution
4:   Transmit  $\hat{I}^{(i)}$  and  $S^{(i)}$  to the server
5:   # Server
6:    $\mathbf{x}^{(i)} \leftarrow f_v(\hat{I}^{(i)})$ ,  $\mathbf{s}^{(i)} \leftarrow \text{Tokenize}(S^{(i)})$             $\triangleright$  Encode global image and sentence
7:   for  $t = 1 : T$  do
8:      $y_t^{(i)} \leftarrow f_l(\mathbf{x}^{(i)}, \mathbf{s}^{(i)}, \mathbf{y}_{<t}^{(i)})$             $\triangleright$  Autoregressive decoding
9:      $g_t^{(i)} \leftarrow g(\mathbf{x}^{(i)}, \mathbf{s}^{(i)}, \mathbf{y}_{<t}^{(i)})$             $\triangleright$  Compute token-level entropy
10:    end for
11:     $G_{\text{avg}} \leftarrow \frac{1}{T} \sum_{t=1}^T g_t^{(i)}$             $\triangleright$  Average entropy over sequence
12:    if  $G_{\text{avg}} \geq \eta$  then
13:       $A_{\text{rel}}^{(i)} \leftarrow \text{Rel\_Att}(\mathbf{x}^{(i)}, \mathbf{s}^{(i)})$             $\triangleright$  Compute relative attention map
14:       $\mathbf{b}^{(i)} \leftarrow \text{Find\_Bbox}(A_{\text{rel}}^{(i)})$             $\triangleright$  Locate bounding box using sliding window
15:      Request cropped image from edge device by transmitting  $\mathbf{b}^{(i)}$ 
16:      # Edge Device
17:       $\tilde{I}^{(i)} \leftarrow \text{Resize}(\text{Crop}(I^{(i)}, \mathbf{b}^{(i)}))$             $\triangleright$  Crop image based on bounding box and resize
18:      Transmit  $\tilde{I}^{(i)}$  to the server
19:      # Server
20:       $\tilde{\mathbf{x}}^{(i)} \leftarrow f_v(\tilde{I}^{(i)})$             $\triangleright$  Encode cropped local image
21:      for  $t = 1 : T$  do
22:         $y_t^{(i)} \leftarrow f_l(\mathbf{x}^{(i)}, \tilde{\mathbf{x}}^{(i)}, \mathbf{s}^{(i)}, \mathbf{y}_{<t}^{(i)})$             $\triangleright$  Refine inference using both global and local features
end if
23:   Return  $\mathbf{y}^{(i)}$  to the client
24: end for

```

---

local image as  $\tilde{\mathbf{x}}^{(i)} = f_v(\tilde{I}^{(i)})$  and performs a second-stage inference using both the global and local features:

$$y_t^{(i)} = f_l(\mathbf{x}^{(i)}, \tilde{\mathbf{x}}^{(i)}, \mathbf{s}^{(i)}, \mathbf{y}_{<t}^{(i)}). \quad (12)$$

The language model then produces the final output sequence  $\mathbf{y}^{(i)}$ , which is transmitted back to the edge device. The proposed framework maintains inference accuracy while reducing communication cost by selectively augmenting local visual inputs only when the model's initial inference is uncertain.

## V. ENTROPY-AWARE IMAGE RETRANSMISSION

We incorporate inference uncertainty into the framework to adaptively balance communication cost and inference accuracy. This framework accounts for the varying difficulty across different image-question pairs. For simple visual scenes or straightforward questions, inference based solely on the global image is often sufficient, eliminating the need for additional edge-server interaction. In contrast, complex scenes or semantically demanding questions require finer-grained visual information. This necessitates transmitting additional image data from the edge to the server, thereby increasing communication cost.

### A. Entropy Metric for VLMs

A critical component of this framework is determining whether the initial inference is reliable or whether additional

image information should be requested. Although the server cannot directly verify correctness, it can estimate the confidence of its prediction from the output probabilities of the LLM decoder. These probabilities are obtained by applying a softmax function to the logits of each generated token. Formally, the softmax output for the  $t$ -th token corresponds to the model's predictive distribution:  $p_\theta(y_t | \mathbf{x}, \mathbf{s}, \mathbf{y}_{<t})$ , where  $\theta$  denotes the LLM parameters. We define an entropy function  $g : \mathbb{R}^E \rightarrow \mathbb{R}$  that maps the softmax distribution over a vocabulary of size  $E$  to a scalar entropy value. For example, in the case of the LLaVA-1.5,  $E = 32,000$  [3], [19].

Because of the autoregressive nature of the LLM, the total uncertainty of a generated sequence can be estimated by aggregating the *token-level* entropy values. The average predictive uncertainty is given by

$$G_{\text{avg}} = \frac{1}{T} \sum_{t=1}^T g(\mathbf{x}, \mathbf{s}, \mathbf{y}_{<t}). \quad (13)$$

If  $G_{\text{avg}}$  exceeds a predefined threshold  $\eta$ , the server requests a retransmission to the edge device. This mechanism ensures that retransmissions occur only when necessary, maintaining reliability while conserving both communication and computational resources.

We measure inference uncertainty using three metrics: 1) Shannon entropy, 2) min-entropy, and 3) probability margin, each associated with its own threshold. The Shannon entropy, a

TABLE I  
NUMBER OF VISUAL TOKENS AND AVERAGE INPUT TOKEN SEQUENCE LENGTH IN TEXTVQA INFERENCE

	Visual Tokens	Average Input Sequence	Proportion of Visual Tokens
Initial Inference	576	605	95.2 %
Second Inference	1152	1181	97.5 %

widely used metric for quantifying uncertainty [14], is defined as

$$g(\mathbf{x}, \mathbf{s}, \mathbf{y}_{<t}) = -\mathbb{E}_{p_\theta(y_t|\mathbf{x}, \mathbf{s}, \mathbf{y}_{<t})} [\log_2 p_\theta(y_t|\mathbf{x}, \mathbf{s}, \mathbf{y}_{<t})], \quad (14)$$

where  $\mathcal{Y}$  denotes the set of all possible output tokens. A high Shannon entropy indicates that the input sequence  $\{\mathbf{x}, \mathbf{s}, \mathbf{y}_{<t}\}$  is challenging for VLM inference, implying lower confidence in the generated response. Therefore, if  $G_{\text{avg}} \geq \eta$ , the server requests a detailed local image to refine the inference result.

The min-entropy provides a conservative measure of uncertainty [13], [34] and is defined as

$$g_m(\mathbf{x}, \mathbf{s}, \mathbf{y}_{<t}) = -\log_2 \max_{y_t \in \mathcal{Y}} p_\theta(y_t|\mathbf{x}, \mathbf{s}, \mathbf{y}_{<t}). \quad (15)$$

As in the Shannon entropy, if  $G_{m,\text{avg}} \geq \eta_m$ , the server requests a local image for refinement.

The final metric, probability margin, measures the gap between the probabilities of the most likely token  $y_{t,1}$  and the second most likely token  $y_{t,2}$  [15]. The probability margin is defined as

$$g_p(\mathbf{x}, \mathbf{s}, \mathbf{y}_{<t}) = p_\theta(y_{t,1}|\mathbf{x}, \mathbf{s}, \mathbf{y}_{<t}) - p_\theta(y_{t,2}|\mathbf{x}, \mathbf{s}, \mathbf{y}_{<t}). \quad (16)$$

In contrast to the other uncertainty metrics, a smaller probability margin indicates lower confidence in the inference result. Accordingly, if  $G_{p,\text{avg}} \leq \eta_p$ , the server requests a local image for refined inference.

We evaluate the effectiveness of different uncertainty metrics by measuring the divergence between the entropy distributions of correct and incorrect samples. As shown in the experimental results in Section VII-C, the min-entropy provides the most reliable criterion for requesting retransmission. Consequently, the entropy-aware image retransmission based on the min-entropy achieves higher communication efficiency at a given level of inference accuracy compared with alternative metrics.

### B. Computational Analysis

The proposed min-entropy-based retransmission strategy not only reduces communication cost but also enhances computational efficiency. We adopt the FLOPs estimation method from [12] to quantify the computation cost during inference. Table I presents the number of visual tokens and the overall token sequence length of LLaVA-1.5 on a TextVQA benchmark [35]. Since visual tokens constitute more than 95 % of the total sequence length in both the initial and secondary inference stages, we focus on the number of visual tokens, denoted as  $n_v$ . As the prefill stage of the LLM decoder typically dominates the overall computational budget when using key-value cache [36], [37], our analysis concentrates on its FLOPs.

For an image-text pair, the FLOPs required for inference can be expressed as a function of the number of visual tokens  $n_v$ :

$$\text{FLOPs}(n_v) = (24n_v d_{\text{LLM}}^2 + 4n_v^2 d_{\text{LLM}}) L, \quad (17)$$

where  $L$  denotes the number of transformer layers in the LLM decoder. Since  $n_v$  (e.g., 576) is typically much smaller than  $d_{\text{LLM}}$  (e.g., 4096) in practical models [3], [38], the overall computational cost scales approximately linearly with  $n_v$ . The FLOPs for the initial inference are given by

$$\text{FLOPs}^{(\text{init})} = \text{FLOPs}(n_v). \quad (18)$$

For the second stage, the total FLOPs comprise both the cost of computing relative attention and the cost of performing inference with doubled visual tokens:

$$\text{FLOPs}^{(\text{2nd})} = \text{FLOPs}(n_v) + \text{FLOPs}(2 \cdot n_v). \quad (19)$$

Here, the computational cost of obtaining the relative attention map is on the same order as that of the initial inference, as the process re-executes the prefill stage with a modified prompt to extract the generic attention map, which will be explained in Section VI. The total computational cost of the proposed framework for a single data sample is:

$$\text{FLOPs} = \begin{cases} \text{FLOPs}^{(\text{init})} & \text{if } G_{\text{avg}} < \eta, \\ \text{FLOPs}^{(\text{init})} + \text{FLOPs}^{(\text{2nd})} & \text{otherwise.} \end{cases} \quad (20)$$

The numerical results in Section V-B confirm that the min-entropy-based retransmission policy not only improves communication efficiency but also achieves a lower expected computational cost than full retransmission, validating its effectiveness along both dimensions.

## VI. ATTENTION-GUIDED COLLABORATIVE VISUAL CROPPING

The proposed framework incorporates attention-guided visual cropping (ViCrop) [11] into the collaborative edge–server inference for VLMs. By identifying semantically important regions in the original image only when necessary, the proposed method maintains the inference accuracy achieved by ViCrop while substantially reducing both communication cost and server-side computational overhead. In this section, we briefly review the ViCrop mechanism and then describe its adaptation to the collaborative edge-to-server inference framework.

### A. Attention-Guided Visual Cropping

ViCrop identifies the RoI in an image by taking into account the model’s attention maps. Recently, the authors of [11] reported that state-of-the-art MLLMs often fail to capture fine-grained visual details—such as small objects or localized regions—due to a perceptual bias toward coarse features. To address this limitation, they proposed scalable, training-free

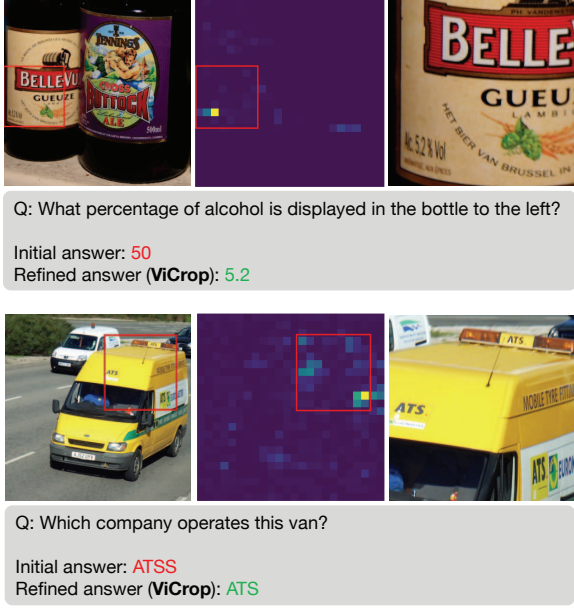


Fig. 3. Visualization of the ViCrop method. The left image shows the original input, the middle image presents the relative attention map corresponding to the given question with the bounding box, and the right image is the detail-preserved local image.

methods for automatic visual localization based on the model’s attention dynamics. A key observation is that even when a VLM produces incorrect answers, it tends to focus on semantically meaningful regions, implicitly indicating where the model *looks*. ViCrop leverages this property to determine the RoI and crop the corresponding area of the original image as an additional input, thereby improving task performance. Examples of original images, attention maps, and cropped local regions obtained by the ViCrop for corresponding questions are shown in Fig. 3.

#### B. ViCrop-Assisted Retransmission Mechanism

The proposed framework integrates ViCrop into its retransmission mechanism, executing it conditionally based on inference uncertainty. Specifically, cropping is performed only when the min-entropy of the initial inference exceeds a pre-defined threshold, ensuring that additional transmissions occur only when necessary. Once activated, the server computes a relative attention map  $A_{\text{rel}}$  and determines a bounding box  $b$  that localizes the RoI. The server then sends a retransmission request along with  $b$  to the edge device. Upon receiving the request, the edge device crops the original image accordingly and resizes the cropped region to match the input resolution of the vision encoder:

$$\tilde{I} = \text{Resize}(\text{Crop}(I, b)). \quad (21)$$

The resulting local image  $\tilde{I}$  is transmitted to the server, which performs a second inference using both the global and local images.

To compute the relative attention map  $A_{\text{rel}}$ , the server extracts attention weights from the LLM decoder’s starting output token directed toward image tokens, yielding an attention tensor  $A_{\text{si}}(\mathbf{x}, \mathbf{s}) \in \mathbb{R}^{L \times H \times 1 \times n_v}$ . The attention values are averaged across all  $H$  heads, and a specific layer

$l \in \{1, \dots, L\}$  is empirically chosen to maximize the contrast between high- and low-attention regions, yielding  $\hat{A}_{\text{si}}^l(\mathbf{x}, \mathbf{s}) \in \mathbb{R}^{1 \times n_v}$ . Following [11], semantic relevance is further enhanced using relative attention, in which the attention for the task-specific query  $\mathbf{s}$  is normalized by that of a generic instruction  $\mathbf{s}'$  (“Write a general description of the image.”):

$$A_{\text{rel}} = \frac{\hat{A}_{\text{si}}^l(\mathbf{x}, \mathbf{s})}{\hat{A}_{\text{si}}^l(\mathbf{x}, \mathbf{s}')} \in \mathbb{R}^{1 \times n_v}. \quad (22)$$

The server then applies a sliding-window search with candidate window sizes (e.g.,  $\{1.0, 1.2, \dots, 2.0\}$  times the input resolution of the vision encoder). For each candidate, the sum of relative attention values within the corresponding window is computed, and the region exhibiting the highest internal-external contrast is selected as the final bounding box.

This collaborative extension of ViCrop transforms a purely accuracy-oriented cropping method in [11] into an integral component of the proposed framework. By integrating entropy-aware retransmission with *server-side RoI estimation* and *edge-side cropping*, the proposed framework transmits semantically critical regions only when necessary. Experimental results presented in the following section demonstrate that this approach substantially reduces both communication and computation costs while maintaining inference accuracy.

## VII. EXPERIMENTAL RESULTS

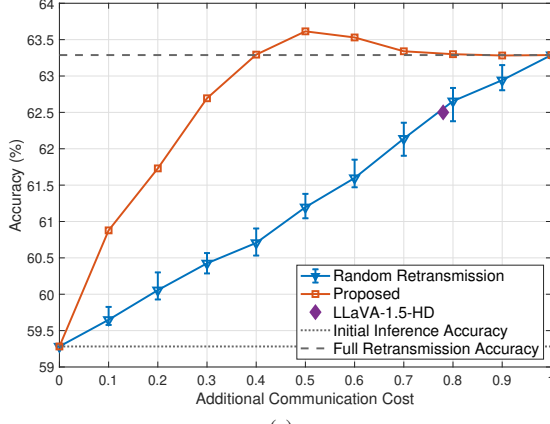
### A. Experiment Settings

We evaluate the proposed edge-to-server inference framework using three state-of-the-art open-source VLMs: LLaVA-1.5 (Vicuna-7B) [3], InstructBLIP [4], and Qwen2.5-VL-7B [5]. These models primarily differ in the input resolution of their vision encoder. Specifically, LLaVA-1.5 and InstructBLIP employ vision encoders with fixed input resolutions of  $336 \times 336$  and  $224 \times 224$  pixels, respectively. In contrast, Qwen2.5-VL adopts a variable-resolution vision encoder. To ensure a consistent comparison, we fix its input resolution to  $224 \times 224$  pixels. We conduct experiments on five widely used VQA benchmark datasets: TextVQA [35], POPE [39], A-OKVQA [40], GQA [41], and VQAv2 [42].

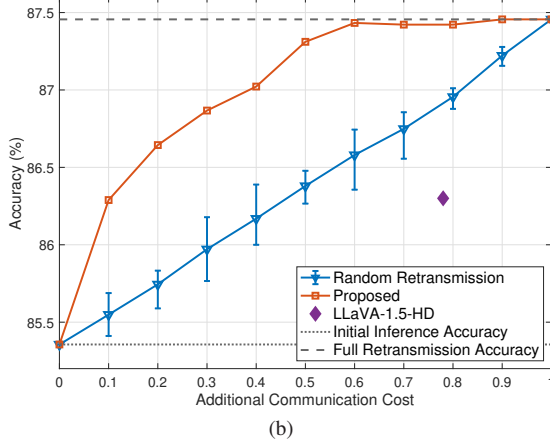
In our experiments, we analyze the tradeoff between the additional communication cost and task accuracy. The additional communication cost is defined as the difference between the total transmitted data and the baseline cost of transmitting all samples as global images. For example, if the server requests local images for all data samples (i.e., the entropy threshold  $\eta$  is set to 0), the additional communication cost equals 1. On the other hand, when the server performs inference only using global images (i.e.,  $\eta \rightarrow \infty$ ), the additional communication cost is 0.

### B. Effectiveness of the Proposed Method

We first evaluate the effectiveness of the proposed framework in terms of communication and computation costs. Fig. 4 presents the tradeoff between communication cost and inference accuracy obtained by the LLaVA-1.5-7B model on TextVQA+OCR and POPE benchmarks. Here, ‘TextVQA+OCR’ refers to the evaluation setting of [3], [35],



(a)

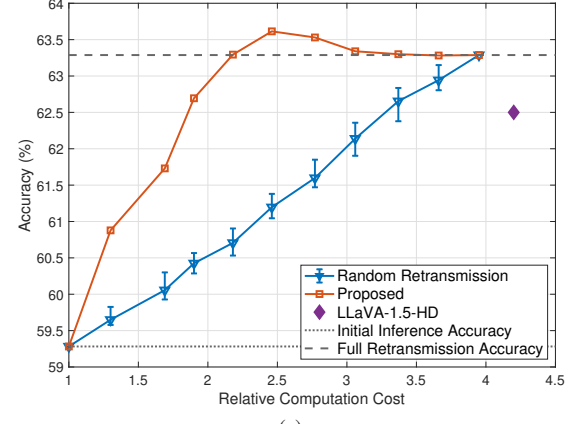


(b)

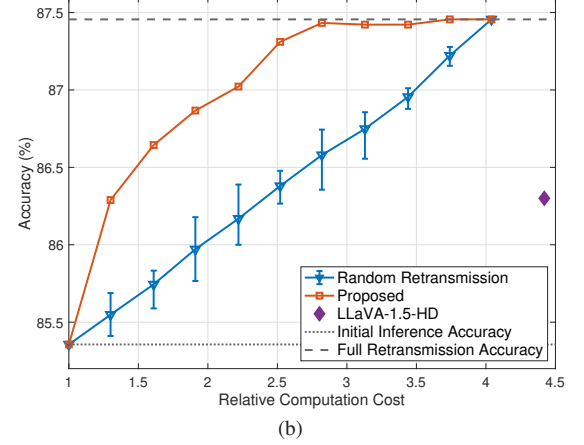
Fig. 4. Tradeoff between communication cost and inference accuracy for the LLaVA-1.5-7B model on (a) TextVQA+OCR and (b) POPE benchmarks. The entropy metric used is min-entropy. The proposed framework achieves a more favorable communication-accuracy tradeoff compared with the high-resolution model variant (LLaVA-1.5-HD) and the random retransmission baseline.

in which OCR tokens extracted from the image are appended to the VLM’s input text [11]. The dotted line labeled *initial inference accuracy* denotes the accuracy when only single-stage transmission is performed, whereas *full retransmission accuracy* line represents the accuracy when all samples are retransmitted in the two-stage scheme. The results are compared with those of the high-resolution variant model, LLaVA-1.5-HD (Vicuna-13B) [3], which scales to  $448 \times 448$  images by splitting them into multiple sub-images for the vision encoder and concatenating an additional downsampled thumbnail image as context. The purple diamond marker indicates the achievable point reported for LLaVA-1.5-HD in [3]. We also include *random retransmission* as a baseline, in which local images are retransmitted randomly without considering sample-level uncertainty. For fairness of comparison, ViCrop is applied to the randomly selected samples to generate local images in the same manner as in the proposed method. Fig. 5 further shows the tradeoff between computation cost and inference accuracy. Here, the relative computation cost is defined as the ratio of the total computational load to that required for performing the initial inference on the entire dataset using LLaVA-1.5-7B.

The experimental results demonstrate the advantages of the



(a)



(b)

Fig. 5. Tradeoff between computation cost and inference accuracy for the LLaVA-1.5-7B model on (a) TextVQA+OCR and (b) POPE benchmarks. The entropy metric used is min-entropy. The proposed framework achieves a more favorable computation-accuracy tradeoff compared with the high-resolution model variant (LLaVA-1.5-HD) and the random retransmission baseline.

proposed method in two key aspects. First, it achieves higher inference accuracy at lower communication costs. As shown in Fig. 4(a) and Fig. 4(b), the proposed method outperforms LLaVA-1.5-HD while incurring only 0.28 and 0.1 additional communication cost, respectively, which is substantially lower than the 0.78 required by LLaVA-1.5-HD. Second, although LLaVA-1.5-HD employs a language model with nearly twice as many parameters as LLaVA-1.5-7B used in the proposed framework (13B vs. 7B), our method achieves higher accuracy while significantly reducing server-side computational and memory requirements. As shown in Fig. 5, the proposed method achieves comparable or superior accuracy with significantly lower computational costs compared to LLaVA-1.5-HD.

### C. Choice of Uncertainty Metric

In this subsection, we investigate which entropy metric provides the most effective tradeoff between task accuracy and communication cost. As shown in Fig. 6, we compare the performance of three uncertainty-based retransmission strategies—Shannon entropy, min-entropy, and probability margin—against a random retransmission baseline. The results indicate that uncertainty-aware retransmission substantially

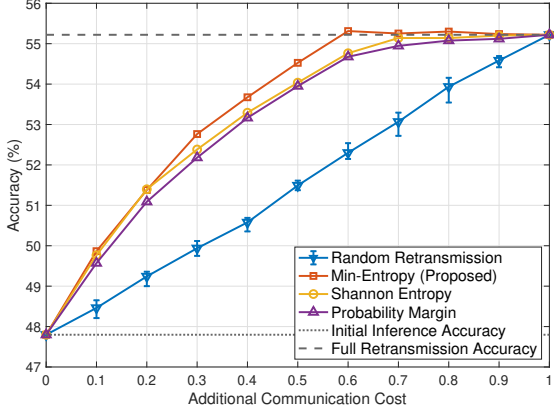


Fig. 6. Comparison of uncertainty metrics for LLaVA-1.5-7B model on TextVQA benchmark. We aggregate token-level entropy over the entire output sequence. The min-entropy-based retransmission strategy shows the best accuracy-communication cost tradeoff compared with other uncertainty metrics.

TABLE II

STATISTICAL DISTANCES BETWEEN ENTROPY DISTRIBUTIONS OF CORRECT AND INCORRECT SAMPLES

	Min-Entropy	Shannon Entropy	Prob. Margin
Overlap ( $\downarrow$ )	<b>0.47</b>	0.54	0.49
$D_B$ ( $\uparrow$ )	<b>0.33</b>	0.27	0.24

outperforms random retransmission, achieving accuracy comparable to the full retransmission setting with only 60 % of the additional communication cost. Among the uncertainty metrics evaluated, min-entropy consistently provides the best performance across most operating points.

Table II reports the separability between the uncertainty distributions of correct and incorrect predictions produced by the LLaVA-1.5-7B model on the TextVQA benchmark, evaluated using three different uncertainty estimation methods. To quantify this separability between two distributions, we employ two metrics: the distribution overlap and the Bhattacharyya distance ( $D_B$ ) [43]. Given two probability mass functions (PMF)  $p(x)$  and  $q(x)$ , these metrics are defined as:

$$\text{Overlap}(p, q) = \sum_x \min(p(x), q(x)), \quad (23)$$

$$D_B(p, q) = -\ln \sum_x \sqrt{p(x)q(x)}. \quad (24)$$

A lower overlap and a higher Bhattacharyya distance indicate stronger separability between the uncertainty distributions of correct and incorrect predictions. As shown in Table II, the min-entropy achieves the lowest overlap and the highest Bhattacharyya distance among the three metrics, showing the most pronounced distributional separation. This observation is consistent with Fig. 6, where the min-entropy achieves the most favorable accuracy-communication cost tradeoff. These findings confirm that the min-entropy is the most discriminative uncertainty measure for our collaborative inference framework.

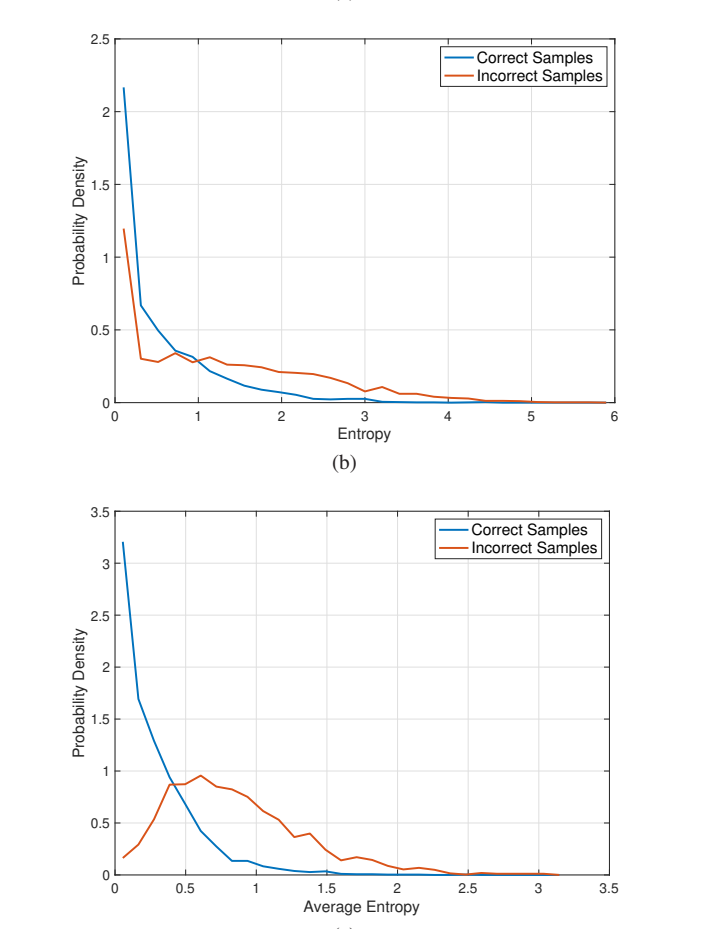
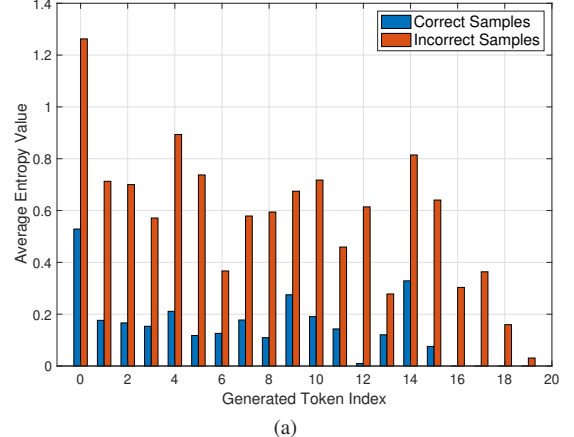


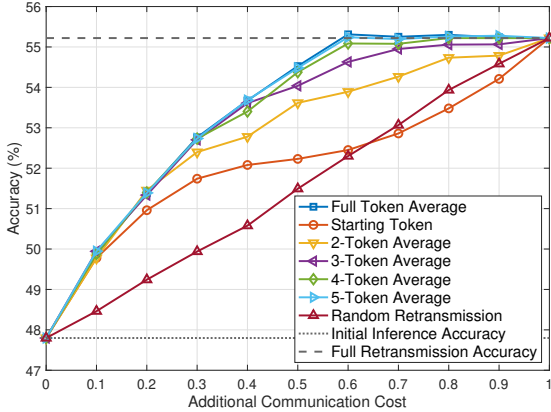
Fig. 7. Analysis of min-entropy aggregation on TextVQA benchmark. (a) Average min-entropy at each generation step for correct and incorrect samples, (b) min-entropy distribution of the starting token, and (c) min-entropy distribution of the full-sequence average.

#### D. Uncertainty Aggregation Strategy

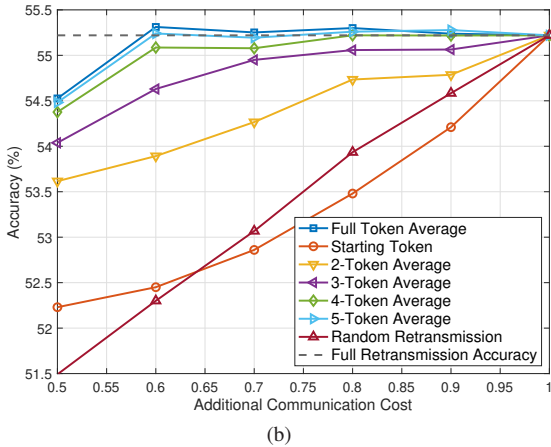
We analyze the effectiveness of token-level entropy as a measure of VLM inference uncertainty and investigate how to aggregate token-wise values into a sequence-level uncertainty score. First, we statistically compare the token-level min-entropy of correct and incorrect predictions produced by the LLaVA-1.5-7B model on the TextVQA benchmark. Fig. 7(a) shows the average min-entropy value at each generation step, where the maximum output length is set to 20 tokens. Incorrect

TABLE III  
STATISTICAL DISTANCES BETWEEN ENTROPY DISTRIBUTIONS OF  
CORRECT AND INCORRECT SAMPLES UNDER TOKEN AGGREGATION

	Starting Token	Full Token Average
Overlap ( $\downarrow$ )	0.63	<b>0.47</b>
$D_B$ ( $\uparrow$ )	0.19	<b>0.33</b>



(a)

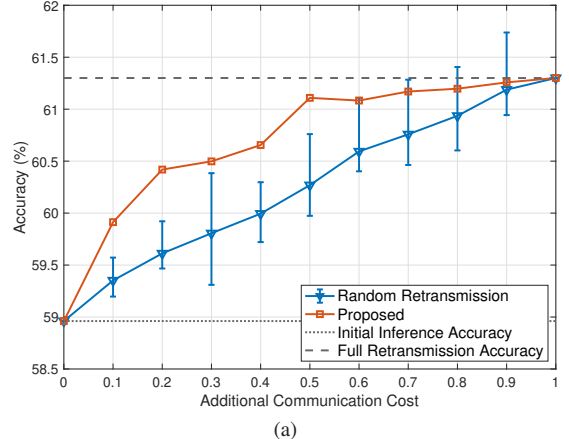


(b)

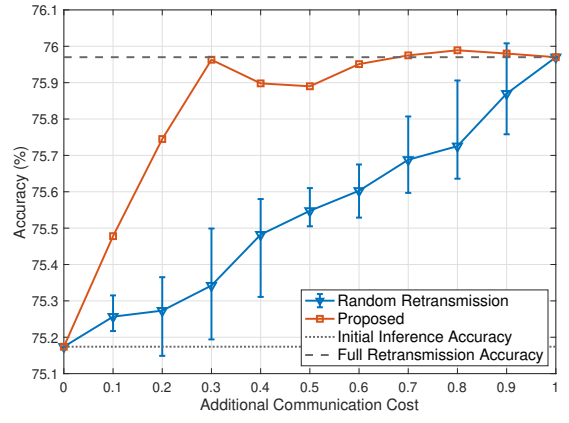
Fig. 8. Comparison of tradeoff curves for different token aggregation lengths. (a) shows the overall tradeoff, while (b) zooms in on the region of interest, focusing on the high-accuracy regime.

samples consistently exhibit higher min-entropy across all token positions. In contrast, correct samples maintain lower min-entropy values, indicating more confident predictions throughout the sequence. This clear separation shows that token-level min-entropy provides meaningful cues for distinguishing correct from incorrect predictions.

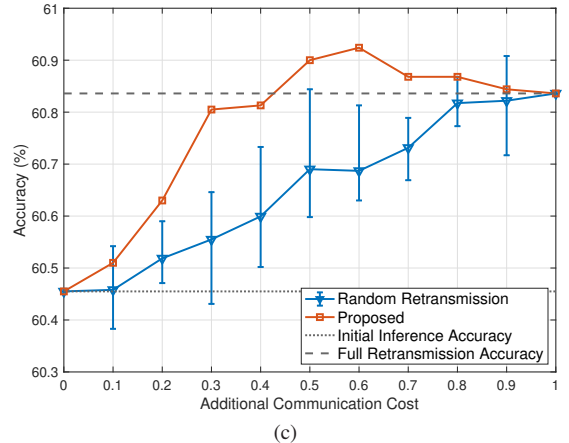
Fig. 7(b) and Fig. 7(c) compare the min-entropy distributions of the starting token and the full-sequence average, respectively. In Fig. 7(b), a considerable fraction of incorrect samples show the min-entropy values close to zero, which is less evident in Fig. 7(c). Table III quantifies this effect: starting-token min-entropy exhibits higher overlap and lower Bhattacharyya distance, reflecting weaker discriminative power compared to full-sequence averaging. These results confirm that aggregating the min-entropy values across the entire sequence provides a more reliable uncertainty estimate, improving the separation between correct and incorrect predictions. Therefore, full-sequence min-entropy aggregation—rather



(a)



(b)



(c)

Fig. 9. Tradeoff between additional communication cost and task accuracy for LLaVA-1.5-7B across different benchmarks: (a) A-OKVQA, (b) VQAv2, and (c) GQA.

than relying solely on a starting token alone—provides a more accurate uncertainty estimate for the proposed collaborative inference.

To further examine the influence of the aggregation length, we analyze how task accuracy varies with the number of tokens included in the entropy average. Fig. 8 shows the tradeoff between task accuracy and communication cost as a function of aggregation length, where the “ $i$ -token average” refers to using the min-entropy averaged over the first  $i$  generated tokens to determine whether retransmission is necessary.

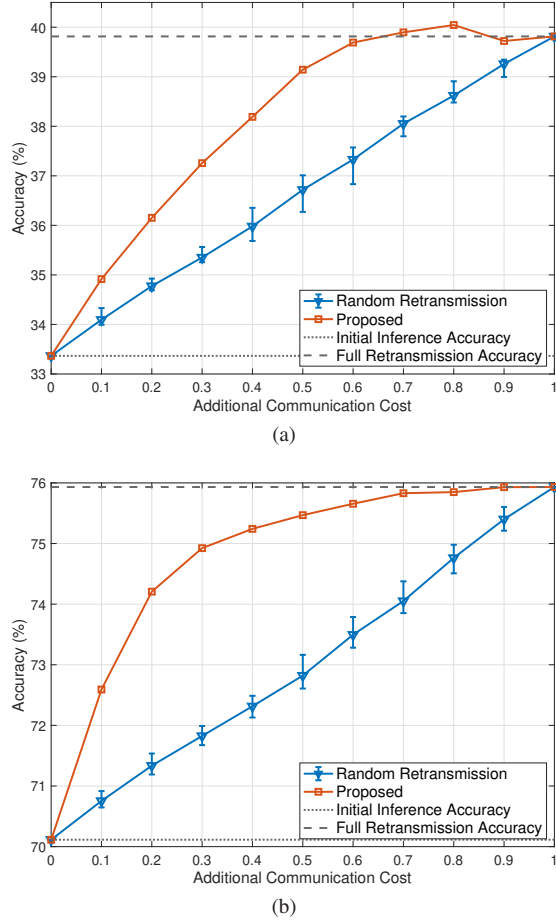


Fig. 10. Tradeoff between additional communication cost and task accuracy on TextVQA benchmark across different VLM architectures: (a) InstructBLIP and (b) Qwen2.5-VL.

Notably, averaging over only the first five tokens achieves performance comparable to full-sequence aggregation, indicating that a limited number of initial tokens often suffices to characterize inference uncertainty without requiring full-sequence generation in the first stage.

#### E. Effectiveness Across Datasets and VLM Architectures

We demonstrate the practical usefulness of the proposed method through experiments on multiple datasets and VLM architectures. Fig. 9 presents the experimental results on A-OKVQA, VQAv2, and GQA, three widely used benchmarks for evaluating visual reasoning and conceptual understanding [40]–[42]. Across these datasets, the proposed method effectively improves inference accuracy for a given communication budget compared with random retransmission. Fig. 10 evaluates the proposed method on InstructBLIP [4] and Qwen2.5-VL [5]. For these models, our method achieves higher accuracy at the same communication cost, confirming that the approach remains effective for different VLM architectures.

#### F. Compatibility with Image Compression

The proposed method also shows strong compatibility with image compression techniques, enabling additional reductions



Fig. 11. Visualization of global and local images combined with image compression: (a) the original image, (b) the compressed global image using JPEG quality 5, (c) the magnified ROI corresponding to the red bounding box in (b), and (d) the compressed local image using the same JPEG quality as in (b).

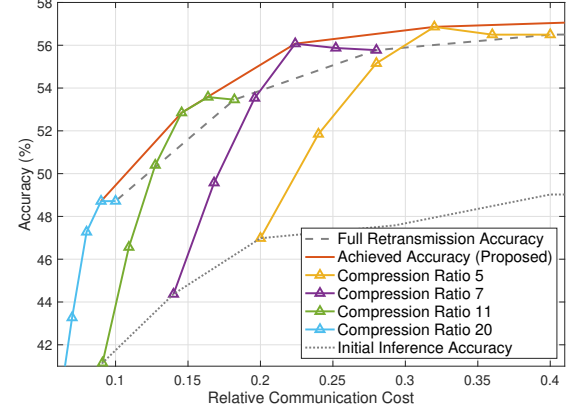


Fig. 12. Additional gain achieved by combining the proposed method with JPEG image compression. Results are evaluated using LLaVA-1.5-7B on the TextVQA benchmark.

in communication cost. Fig. 11 illustrates that, even under severe compression, the proposed framework effectively preserves the visual details within the VLM’s ROI. Fig. 11(a) displays the original image, and Fig. 11(b) shows the corresponding compressed global image with JPEG quality set to 5. Fig. 11(c) provides a magnified view of the red bounding box in Fig. 11(b), highlighting the ROI. Fig. 11(d) presents the local image identified by ViCrop and compressed using the same JPEG quality. Compared with Fig. 11(c), the local image in Fig. 11(d) retains sharper visual details and mitigates the accuracy degradation typically caused by image compression, confirming the effectiveness of the proposed framework.

Fig. 12 shows the accuracy–communication tradeoff under different compression ratios, where the relative communication cost is defined as the ratio of the transmitted data size of a compressed image to that of a JPEG global image encoded at

quality 100. By integrating the proposed method with image compression, further communication savings can be obtained; for instance, the relative communication cost is reduced to 0.25 while maintaining a task accuracy of 56.5%, compared with the 0.40 required by full retransmission.

### VIII. CONCLUSION

We proposed a novel collaborative edge-to-server inference framework that leverages pre-trained VLMs. In the initial inference stage, the server performs inference on a global image transmitted from the edge device and identifies task-relevant regions based on the model's internal attention. The reliability of this initial inference is assessed using the min-entropy of output tokens. When the min-entropy exceeds a predefined threshold, a second-stage inference is triggered using both global and local images.

Experimental results show that the proposed framework significantly reduces communication and computation overhead while maintaining inference accuracy relative to baseline methods. The proposed method remains effective across diverse VQA tasks and VLM architectures. Furthermore, its combination with existing image compression techniques enables additional communication savings. Future work will explore extending the framework to more complex communication settings, including robust transmission and multi-access environments.

### REFERENCES

- [1] A. Radford, J. W. Kim, C. Hallacy, A. Ramesh, G. Goh, S. Agarwal, G. Sastry, A. Askell, P. Mishkin, J. Clark *et al.*, “Learning transferable visual models from natural language supervision,” in *Proc. Int. Conf. Mach. Learn. (ICML)*, Jul. 2021, pp. 8748–8763.
- [2] J. Zhang, J. Huang, S. Jin, and S. Lu, “Vision-language models for vision tasks: a survey,” *IEEE Trans. Pattern Anal. Mach. Intell.*, vol. 46, no. 8, pp. 5625–5644, Feb. 2024.
- [3] H. Liu, C. Li, Y. Li, and Y. J. Lee, “Improved baselines with visual instruction tuning,” in *Proc. IEEE Conf. Comput. Vis. Pattern Recognition (CVPR)*, Jun. 2024, pp. 26 296–26 306.
- [4] W. Dai, J. Li, D. Li, A. M. H. Tiong, J. Zhao, W. Wang, B. Li, P. Fung, and S. Hoi, “InstructBLIP: Towards general-purpose vision-language models with instruction tuning,” in *Proc. Adv. Neural Inf. Process. Syst. (NeurIPS)*, Dec. 2023, pp. 49 250–49 267.
- [5] S. Bai, K. Chen, X. Liu, J. Wang, W. Ge, S. Song, K. Dang, P. Wang, S. Wang, J. Tang *et al.*, “Qwen2.5-VL technical report,” *arXiv preprint arXiv:2502.13923*, Mar. 2025.
- [6] A. Sharshar, L. U. Khan, W. Ullah, and M. Guizani, “Vision-language models for edge networks: A comprehensive survey,” *IEEE Internet Things J.*, vol. 12, Jun. 2025.
- [7] C. Yuan, Z. Liu, J. Lv, J. Shao, Y. Jiang, J. Zhang, and X. Li, “Task-oriented feature compression for multimodal understanding via device-edge co-inference,” *arXiv preprint arXiv:2503.12926*, Mar. 2025.
- [8] Y. Zhang, H. Wang, Q. Bai, H. Liang, P. Zhu, G.-M. Muntean, and Q. Li, “VaVLM: Toward efficient edge-cloud video analytics with vision-language models,” *IEEE Trans. Broadcast.*, vol. 71, no. 2, pp. 529–541, Apr. 2025.
- [9] A. Dosovitskiy, L. Beyer, A. Kolesnikov, D. Weissenborn, X. Zhai, T. Unterthiner, M. Dehghani, M. Minderer, G. Heigold, S. Gelly *et al.*, “An image is worth 16x16 words: Transformers for image recognition at scale,” in *Proc. Int. Conf. Learn. Representations (ICLR)*, Jun. 2021.
- [10] X. Zhai, B. Mustafa, A. Kolesnikov, and L. Beyer, “Sigmoid loss for language image pre-training,” in *Proc. IEEE Int. Conf. Comput. Vis. (ICCV)*, Sep. 2023, pp. 11 975–11 986.
- [11] J. Zhang, M. Khayatkhoei, P. Chhikara, and F. Ilievski, “MLLMs know where to look: Training-free perception of small visual details with multimodal LLMs,” in *Proc. Int. Conf. Learn. Representations (ICLR)*, Apr. 2025.
- [12] V. A. Korthikanti, J. Casper, S. Lym, L. McAfee, M. Andersch, M. Shoeybi, and B. Catanzaro, “Reducing activation recomputation in large transformer models,” in *MLSys*, Jan. 2023.
- [13] R. Konig, R. Renner, and C. Schaffner, “The operational meaning of min- and max-entropy,” *IEEE Trans. Inf. Theory*, vol. 55, no. 9, pp. 4337–4347, Sep. 2009.
- [14] C. E. Shannon, “A mathematical theory of communication,” *Bell Syst. Tech. J.*, vol. 27, no. 3, pp. 379–423, Jul. 1948.
- [15] B. Settles, *Active Learning*. San Rafael, CA, USA: Morgan & Claypool Publishers, 2012.
- [16] H. Touvron, L. Martin, K. Stone, P. Albert, A. Almairi, Y. Babaei, N. Bashlykov, S. Batra, P. Bhargava, S. Bhosale *et al.*, “Llama 2: Open foundation and fine-tuned chat models,” *arXiv preprint arXiv:2307.09288*, 2023.
- [17] T. Mesnard, C. Hardin, R. Dadashi, S. Bhupatiraju, S. Pathak, L. Sifre, M. Rivière, M. S. Kale, J. Love *et al.*, “Gemma: Open models based on Gemini research and technology,” *arXiv preprint arXiv:2403.08295*, Mar. 2024.
- [18] W.-L. Chiang, Z. Li, Z. Lin, Y. Sheng, Z. Wu, H. Zhang, L. Zheng, S. Zhuang, Y. Zhuang, J. E. Gonzalez, I. Stoica, and E. P. Xing, “Vicuna: An open-source chatbot impressing GPT-4 with 90%\* chatGPT quality,” Mar. 2023. [Online]. Available: <https://lmsys.org/blog/2023-03-30-vicuna/>
- [19] T. Kudo and J. Richardson, “Sentencepiece: A simple and language independent subword tokenizer and detokenizer for neural text processing,” in *Proc. Conf. Empir. Methods Nat. Lang. Process. (EMNLP)*, Nov. 2018, pp. 66–71.
- [20] A. Vaswani, N. Shazeer, N. Parmar, J. Uszkoreit, L. Jones, A. N. Gomez, L. Kaiser, and I. Polosukhin, “Attention is all you need,” in *Proc. Adv. Neural Inf. Process. Syst. (NeurIPS)*, Dec. 2017, pp. 5998–6008.
- [21] J. Im, N. Kwon, T. Park, J. Woo, J. Lee, and Y. Kim, “Attention-aware semantic communications for collaborative inference,” *IEEE Internet Things J.*, vol. 11, no. 22, pp. 37 008–37 020, Nov. 2024.
- [22] J. Park, Y. Oh, Y. Kim, and Y.-S. Jeon, “Vision transformer-based semantic communications with importance-aware quantization,” *IEEE Internet Things J.*, vol. 12, pp. 35 662–35 677, Jun. 2025.
- [23] L. Chen, H. Zhao, T. Liu, S. Bai, J. Lin, C. Zhou, and B. Chang, “An image is worth 1/2 tokens after layer 2: Plug-and-play inference acceleration for large vision-language models,” in *Proc. European Conf. Comput. Vis. (ECCV)*, Oct. 2024, pp. 19–35.
- [24] Q. Zhang, A. Cheng, M. Lu, R. Zhang, Z. Zhuo, J. Cao, S. Guo, Q. She, and S. Zhang, “Beyond text-visual attention: Exploiting visual cues for effective token pruning in VLMs,” in *Proc. IEEE Int. Conf. Comput. Vis. (ICCV)*, Oct. 2025.
- [25] D. Gündüz, Z. Qin, I. E. Aguerri, H. S. Dhillon, Z. Yang, A. Yener, K. K. Wong, and C.-B. Chae, “Beyond transmitting bits: Context, semantics, and task-oriented communications,” *IEEE J. Sel. Areas Commun.*, vol. 41, no. 1, pp. 5–41, Jan. 2023.
- [26] G. Shi, Y. Xiao, Y. Li, and X. Xie, “From semantic communication to semantic-aware networking: Model, architecture, and open problems,” *IEEE Commun. Mag.*, vol. 59, no. 8, pp. 44–50, Aug. 2021.
- [27] Q. Lan, D. Wen, Z. Zhang, Q. Zeng, X. Chen, P. Popovski, and K. Huang, “What is semantic communication? A view on conveying meaning in the era of machine intelligence,” *J. Commun. Inf. Netw.*, vol. 6, no. 4, pp. 336–371, Dec. 2021.
- [28] D. Huang, F. Gao, X. Tao, Q. Du, and J. Lu, “Toward semantic communications: Deep learning-based image semantic coding,” *IEEE J. Sel. Areas Commun.*, vol. 41, no. 1, pp. 55–71, 2022.
- [29] H. Xie and Z. Qin, “A lite distributed semantic communication system for internet of things,” *IEEE J. Sel. Areas Commun.*, vol. 39, no. 1, pp. 142–153, Jan. 2020.
- [30] G. Zhang, Q. Hu, Z. Qin, Y. Cai, G. Yu, and X. Tao, “A unified multi-task semantic communication system for multimodal data,” *IEEE Trans. Commun.*, vol. 72, no. 7, pp. 4101–4116, Feb. 2024.
- [31] L. Huang, W. Yu, W. Ma, W. Zhong, Z. Feng, H. Wang, Q. Chen, W. Peng, X. Feng, B. Qin *et al.*, “A survey on hallucination in large language models: Principles, taxonomy, challenges, and open questions,” *ACM Trans. Inf. Syst.*, vol. 43, no. 2, pp. 1–55, Jan. 2025.
- [32] E. Fadeeva, A. Rubashevskii, A. Shelmanov, S. Petrakov, H. Li, H. Mubarak, E. Tsymbalov, G. Kuzmin, A. Panchenko, T. Baldwin, P. Nakov, and M. Panov, “Fact-checking the output of large language models via token-level uncertainty quantification,” in *Proc. Annu. Meeting Assoc. Comput. Linguistics (ACL)*, Aug. 2024, pp. 9367–9385.
- [33] N. Gupta, H. Narasimhan, A. S. Rawat, W. Jitkrittum, A. Menon, and S. Kumar, “Language model cascades: Token-level uncertainty and beyond,” in *Proc. Int. Conf. Learn. Representations (ICLR)*, May 2024.

- [34] Y. Kim, C. Guyot, and Y.-S. Kim, “On the efficient estimation of min-entropy,” *IEEE Trans. Inf. Forensics Security*, vol. 16, pp. 3013–3025, Apr. 2021.
- [35] A. Singh, V. Natarajan, M. Shah, Y. Jiang, X. Chen, D. Batra, D. Parikh, and M. Rohrbach, “Towards VQA models that can read,” in *Proc. IEEE Conf. Comput. Vis. Pattern Recognition (CVPR)*, Jun. 2019, pp. 8317–8326.
- [36] G.-I. Yu, S. J. Joo, G.-W. Kim, S. Kim, and B.-G. Chun, “Orca: A distributed serving system for Transformer-based generative models,” in *Proc. USENIX Symp. Operating Syst. Design Implementation (OSDI)*, Jul. 2022, pp. 521–538.
- [37] A. Agrawal, N. Kedia, A. Panwar, J. Mohan, N. Kwatra, B. Gulavani, A. Tumanov, and R. Ramjee, “Taming throughput-latency tradeoff in LLM inference with Sarathi-serve,” in *Proc. 18th USENIX Conf. Operating Syst. Design Implement. (OSDI)*, Jul. 2024, pp. 117–134.
- [38] L. Beyer, A. Steiner, A. S. Pinto, A. Kolesnikov, X. Wang, D. Salz, M. Neumann, I. Alabdulmohsin, M. Tschannen, E. Bugliarello *et al.*, “Paligemma: A versatile 3B VLM for transfer,” *arXiv preprint arXiv:2407.07726*, Jul. 2024.
- [39] Y. Li, Y. Du, K. Zhou, J. Wang, W. X. Zhao, and J.-R. Wen, “Evaluating object hallucination in large vision-language models,” in *Proc. Conf. Empir. Methods Nat. Lang. Process. (EMNLP)*, Dec. 2023.
- [40] D. Schwenk, A. Khandelwal, C. Clark, K. Marino, and R. Mottaghi, “A-OKVQA: A benchmark for visual question answering using world knowledge,” in *Proc. European Conf. Comput. Vis. (ECCV)*. Springer, Oct. 2022, pp. 146–162.
- [41] D. A. Hudson and C. D. Manning, “GQA: A new dataset for real-world visual reasoning and compositional question answering,” in *Proc. IEEE Conf. Comput. Vis. Pattern Recognition (CVPR)*, Jun. 2019, pp. 6700–6709.
- [42] Y. Goyal, T. Khot, D. Summers-Stay, D. Batra, and D. Parikh, “Making the V in VQA matter: Elevating the role of image understanding in visual question answering,” in *Proc. IEEE Conf. Comput. Vis. Pattern Recognition (CVPR)*, Jul. 2017, pp. 6904–6913.
- [43] A. Bhattacharyya, “On a measure of divergence between two multinomial populations,” *Sankhya*, vol. 7, no. 4, pp. 401–406, Jul. 1946.